Available online at www.sciencedirect.com
SCIENCE DIRECT
Scripta Materialia 54 (2006) 2149–2153
Scripta MATERIALIA
www.actamat-journals.com

Planar front instabilities during directional solidification of hcp: Zn–Cd dilute alloys

Osvaldo Fornaro *,[1], Hugo A. Palacio [2]

Instituto de Física de Materiales Tandil (IFIMAT), Universidad Nacional del Centro de la Provincia de Buenos Aires, Pinto 399 (B7000GHG) Tandil, Argentina

Received 21 December 2005; received in revised form 15 February 2006; accepted 24 February 2006
Available online 31 March 2006

Abstract

The cellular and dendritic growth of Zn–Cd dilute alloys is directly influenced by crystalline orientation, the primary orientation being the $\langle 10\bar{1}0\rangle$ and eventually $\langle 0001\rangle$. In general, this information is absent during the description of planar to cellular transition. However, it has been experimentally shown that the critical velocity for the stability limit, and the associated wavelength of the first instabilities, are different depending on the growth direction. In this work the stability of the accelerated planar fronts of Zn–0.01%Cd samples, obtained using a Bridgman-like device, and the behavior against morphological stability theory has been compared.

Keywords: Directional solidification; Morphological stability; Cellular growth; Microsegregation

1. Introduction

Microstructure formation during directional solidification of dilute alloys is a very important process, both from an academic point of view and for technological applications. A recent review was given by Boettinger et al. [1]. The morphological stability theory [2–4] defines the conditions under which an initially planar solid–liquid interface could become unstable and therefore form different microstructures.

In the case of dendritic structures, the presence of an anisotropic surface energy allows the structure to define unique operative conditions, fixating the relation between the tip radius and primary spacing. Also, this anisotropy has a fundamental role in the formation of the cellular growth.

Numerous works have been carried out in this way, mainly in face-centered cubic (fcc) crystallography dilute alloys. From them, it is possible to define different morphologies [5–7] as a function of solidification parameters: G_L, thermal gradient at liquid; V, interface advance velocity; C_0, nominal composition of the alloy. For alloys that are more crystallographically complex, the morphology obtained during directional solidification may show a different behavior depending on the growth direction. Besides, a precise description of microstructural evolution does not exist for hexagonal close-packed (hcp) dilute Zn–Cd alloys; only a few descriptions appear in the literature [5,8–10].

For hcp crystals, the preferential growth direction is $\langle 10\bar{1}0\rangle$ as Fig. 1 shows schematically. When the heat extraction does not coincide with this direction, there could be a change in the critical conditions as an effect of that crystalline anisotropy. During planar to cellular transition this results in a change in the critical characteristic values [9–11].

The interfacial energy can be written in three dimensions as

* Corresponding author. Tel.: +54 2293 442 821; fax: +54 2293 444 190.
E-mail address: ofornaro@exa.unicen.edu.ar (O. Fornaro).
[1] Consejo Nacional de Investigaciones Científicas y Técnicas.
[2] Comisión de Investigaciones Científicas de la Provincia de Buenos Aires.

1359-6462/$ - see front matter
doi:10.1016/j.scriptamat.2006.02.049

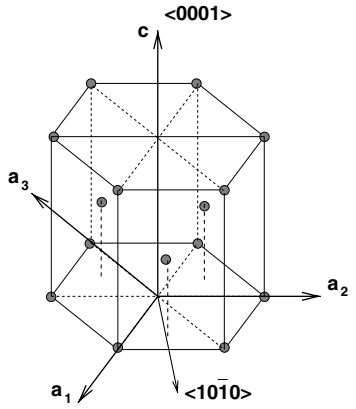

Fig. 1. Crystalline structure of an hcp crystal, where the preferential growth directions $\langle 0001\rangle$ and $\langle 10\bar{1}0\rangle$ are shown.

$$\Gamma(\hat{\mathbf{n}}) = \Gamma_0[1 + \epsilon_0(n_1^4 + n_2^4 + n_3^4)] \quad (1)$$

where Γ_0 is the isotropic part of superficial tension, ϵ_0 indicates the anisotropy degree, which for metals is of the $\approx$0.065 order [12], and $\hat{\mathbf{n}}$ is a unity vector locally normal to the interface.

If we choose, as usual, the $\langle 0001\rangle$ as the azimuthal direction [13] and then measure the relative directions from here, the angular form of the superficial tension $\Gamma(\theta,\phi)$ can be written as a function of the spherical harmonics

$$\Gamma(\theta,\phi) = \Gamma_0[1 + \epsilon_0 Y_{l,m}] \quad (2)$$

Fig. 2 schematically shows the relation $\Gamma(\theta,\phi)/\Gamma_0$ when it is calculated for Y_{33}, assuming a three-fold symmetry in the polar x–y plane [14]. As the figure shows, the relation $\Gamma(\theta,\phi)/\Gamma_0$ can be greater or less than unity in different zones. In particular, a decreasing value of $\Gamma(\theta,\phi)$ appears in the $\langle 0001\rangle$ direction whereas there is an increasing value in the $\langle 10\bar{1}0\rangle$ direction. Physical properties of Zn–Cd alloys used for calculations can be seen in Table 1.

Table 1
Physical properties of Zn–Cd alloys used in the numerical calculations [15]

Liquidus slope	m	−2.8	K/wt.%Cd
Distribution coefficient	k_0	0.13	–
Diffusion coefficient	D_L	3.0×10^{9}	m^2/s
Latent heat of fusion	L	444	J/kg K
Solid thermal conductivity	κ_S	96.0	W/mK
Liquid thermal conductivity	κ_L	164.0	W/mK
Gibbs–Thomson coefficient	Γ	0.7×10^{7}	mK

The fundamental aim of this work was to evaluate some aspects of the microstructure details during the planar to cellular transition, using metallographic analysis of the samples and to extend the classical interpretation of morphological stability approach in order to interpret the experimental results.

2. Experimental

Directional growth of Zn–0.01wt.%Cd alloy was carried out in a Bridgman device. The alloy was prepared starting from Zn (99.999%) and Cd (99.99%) purity materials, carrying out the melting process in a SiC crucible which was painted internally with an alumina coating. Details of the experimental device, as well as the control of the solidification parameters G_L and V, and the procedure of quenching were described previously [16–18]. A schematic illustration of the device is shown in Fig. 3.

The set-up process of the surface for optical microstructural observation and analysis requires great attention, because this alloy can show plastic deformation during the mechanical polishing, giving rise to twinning formation and the re-precipitation of small grains on the surface. To

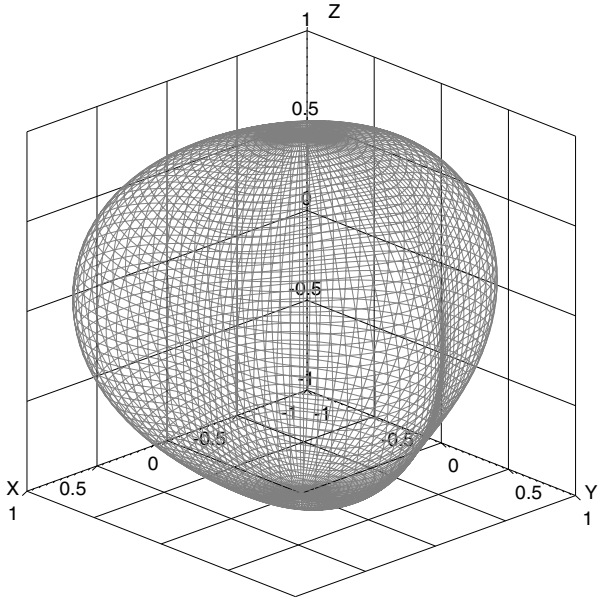

Fig. 2. The relation $(\Gamma(\theta,\phi)/\Gamma_0)$ calculated for hcp crystal.

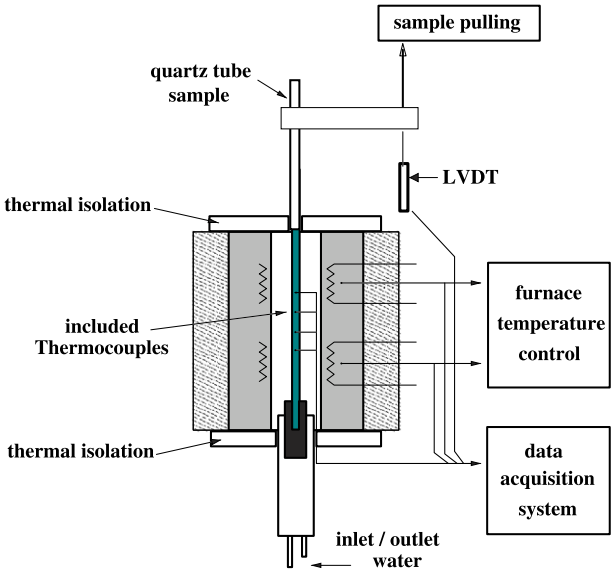

Fig. 3. Schematic view of the experimental device used in this work.

avoid these effects, an extremely slow and continuously refrigerated mechanical polishing was carried out. The microstructure was observed both in longitudinal views (in the direction of the growth) and in cross sections. The surface was set up by mechanical polishing with up to 600 grit SiC abrasive paper, refrigerated with water, and then with 6 and 3 μm diamond powder refrigerated with alcohol. In some cases, chemical polishing with 200 g Na_2CO_3; 6 ml H_2SO_4 in 1000 ml distilled water solution was used for intervals of 1 min. Electrolytic polishing was also used, with 75 ml H_3PO_4 in 625 ml ethanol solution, and 2–5 V direct current; bath temperature less than 10 °C. Electro-polishing also generates a thick surface oxide which allows us to detect changes in crystallographic orientation, when observed under polarized light.

3. Results

It is known that, from a qualitative point of view, for a given composition in an alloy with partition coefficient $k_0 < 1$, there exists a critical value for $\left(\frac{G_L}{VC_0}\right)$ which is given for the modified constitutional supercooling that predicts the limit for a planar–cellular transition. When this relation becomes smaller than the critical, a planar microstructure could evolve to a non planar one, where richer zones correspond to interface depressions. Even for very dilute alloys, the concentration in such depressions could achieve the eutectic composition [19,20].

Once the thermal gradient was fixed at $G_L = 25$ K/cm, we start the experiments by the stabilization of growth below the critical velocity, usually 50 μm/s was chosen for this starting velocity. After a time growing at this velocity, not less than $\tau = D_L/kV^2$, the velocity was increased until it reached the desired value. Fig. 4a shows a photographic composition of the interface for a sample grown at $V = 65$ μm/s, where two grains can be easily identified. It may be noted that the critical wavelength of each grain is different. It is also apparent that planar morphology survives a longer time in the grain on the left, advancing a space of several microns in planar form over the other. Fig. 4b shows a similar situation for a sample obtained at $V = 75$ μm/s. In this case, the difference at the breakdown is not as evident as in Fig. 4a. Critical wavelengths and primary spacing after stabilization were determined from the micrographs.

4. Planar front stability

It is accepted that the growth morphology can be interpreted from the morphological stability theory as a first approximation [1,4–6]. Firstly, we assume that an initially planar front is growing in the z direction with velocity V. This planar front is perturbed by a spatio-temporal function

$$z = \delta \exp\left(\sigma t + i2\frac{\pi x}{\lambda}\right) \tag{3}$$

where δ is the amplitude and λ is the wavelength of the perturbation. The growth rate σ can be determined by resolving the heat and diffusion equations for small δ, where linear expansion of coefficients can be applied [5]. This

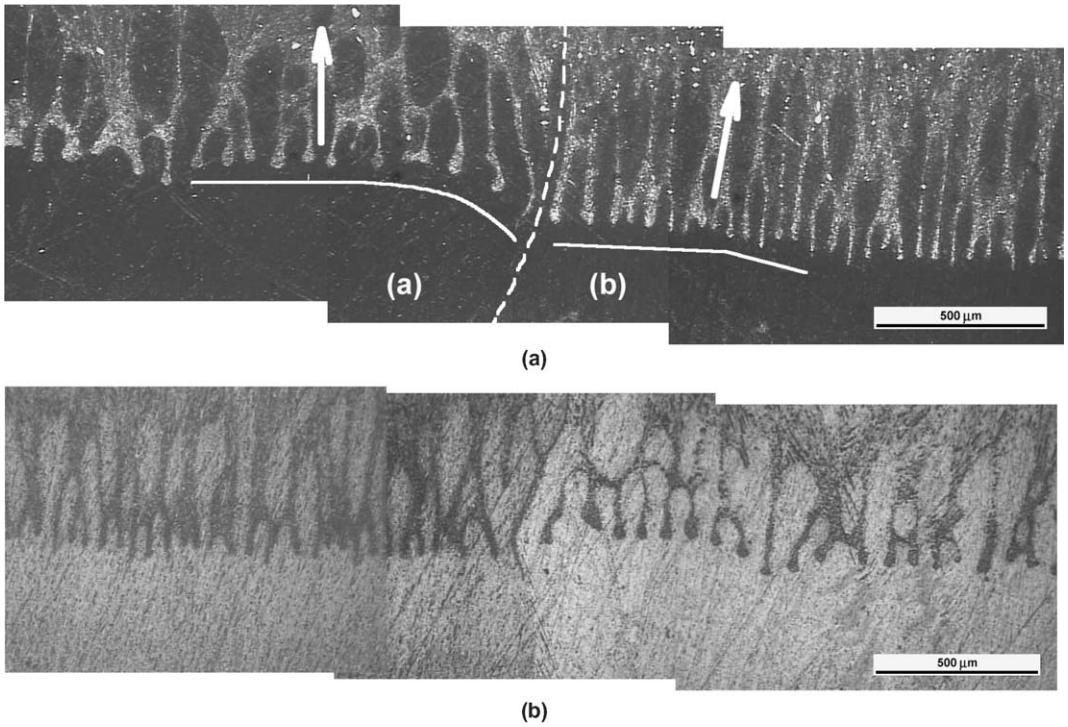

Fig. 4. Micrographs of planar front, Zn–0.01wt.%Cd, $G_L = 25$ K/cm. Samples grown at (a) $V = 65$ μm/s and (b) $V = 75$ μm/s.

calculus results in a function that includes three terms with thermal, diffusive and capillary contributions:

$$\sigma = m_L G_C \xi_C - G - \frac{4\pi^2 T_m \Gamma(\theta,\phi)}{\lambda^2} \quad (4)$$

Negative values of σ for all λ determine a stable planar front, positive values determine an unstable condition and the particular case $\sigma = 0$ defines the limit between stability and instability and then it is called marginal stability. In Eq. (4), T_m corresponds to the solvent equilibrium melting temperature, $\Gamma(\theta,\phi)$ is the Gibbs coefficient, which now has an angular dependence in relation to $\langle 0001\rangle$ direction and G is a thermal gradient, averaged between solid and liquid with the thermal conductivities and it is given by

$$G = \left(\frac{\kappa_S G_S + \kappa_L G_L}{2\bar{\kappa}}\right) \quad (5)$$

where $\bar{\kappa} = (\kappa_S + \kappa_L)/2$ is the average of solid and liquid thermal conductivities. G_C is the composition gradient, which for a planar front advancing at constant velocity can be written as

$$G_C = \left(\frac{VC_0(k_0 - 1)}{k_0 D_L}\right) \quad (6)$$

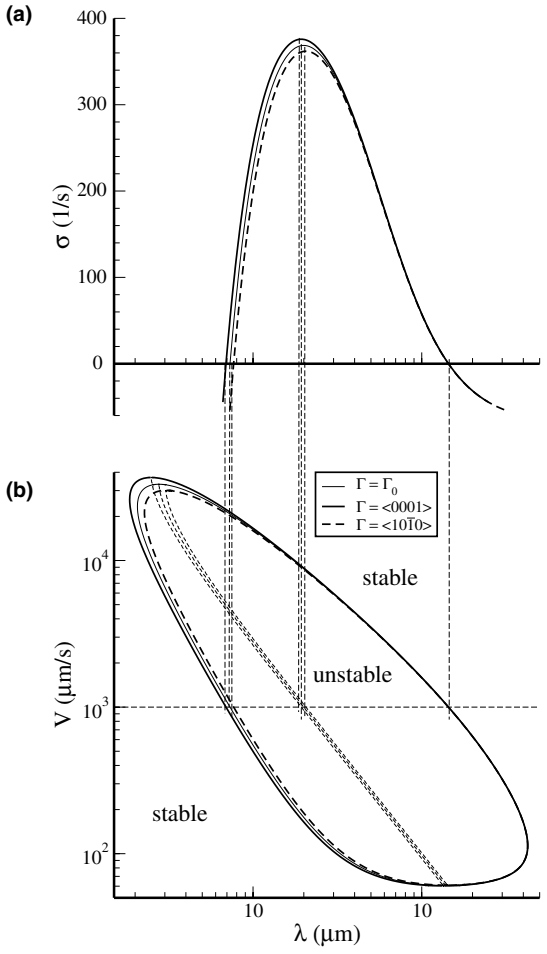

Fig. 5. Stability map generated for Zn–0.01%Cd and a thermal gradient $G_L = 25$ K/cm.

while ξ_C is a parameter which depends on V and λ, that remains close to unity, except at rapid solidification conditions [5], and can be written as

$$\xi_C = 1 + \frac{2k_0}{1 - 2k_0 - \sqrt{1 + \left(\frac{4\pi D_L}{V\lambda}\right)^2}} \quad (7)$$

For a given growth velocity between V_C (modified constitutional supercooling) and V_{abs} (absolute stability criterion), σ is positive for a wavelength interval [5,21], and shows a maximum σ_{max} for an intermediate wavelength $\lambda_{\sigma_{max}}$, as can be seen in Fig. 5a. The wavelengths λ_0^+ and λ_0^-, for which $\sigma = 0$, define the marginal stability condition. Intermediate wavelengths between λ_0^- and λ_0^+ have a propagation rate $\sigma > 0$ and therefore, $\lambda_0^\pm$ limit the instability–stability zone for the planar front. In Fig. 5b the values of λ for which $\sigma = 0$ have been transported for the velocity range among V_C and V_{abs}. As explained after Fig. 2, the calculation was made for $\Gamma_{\langle 10\bar{1}0\rangle}$ and $\Gamma_{\langle 0001\rangle}$, where we expect the maximum differences, and for the neutral Γ_0, for comparison.

5. Discussion

As was seen previously, Eq. (4) together with (5)–(7), allows us to interpret the planar front behavior. In these equations, the angular dependence of $\Gamma(\theta,\phi)$ given by (2) was assumed. This approximation only takes into account that the misorientation of heat flux and primary growth direction only affects supercooling through surface energy and not from kinetic attachment.

Fig. 5 shows a stability map that was calculated for a composition of Zn–0.01wt.%Cd and a thermal gradient $G_L = 25$ K/cm. In Fig. 5a the value of σ is calculated for an intermediate velocity. In this figure, the values of λ_0^+ and λ_0^-, where $\sigma = 0$, and $\lambda_{\sigma_{max}}$, for which σ has a maximum value, are identified and transferred to obtain Fig. 5b. It can be noted that the correction is more evident for the smaller wavelengths and is practically negligible for the greater ones, because the capillary term depends on (λ^{-2}). The correction is also more appreciable at greater velocities. From both figures, it can be seen that the correction is a shift of critical values as $\Gamma(\theta,\phi)$ becomes greater or less than Γ_0.

To interpret the experimental results, Fig. 6 shows the low velocity zone of the stability map, where measured determinations are added. In this figure, minimal λ_{min} and primary spacing λ_1 are indicated. The primary spacing appears after an initial competition and a stabilization process. From the figure, it is evident that there are two well differentiated sets of experimental data points, characterized by the different crystalline orientations of each grain.

In both cases, λ_1 is close to the $\lambda_{\sigma_{max}}$ line, for both data sets. At the same time, λ_{min} remains close to the λ_0^- value, which is in agreement with observations made in Al–Cu

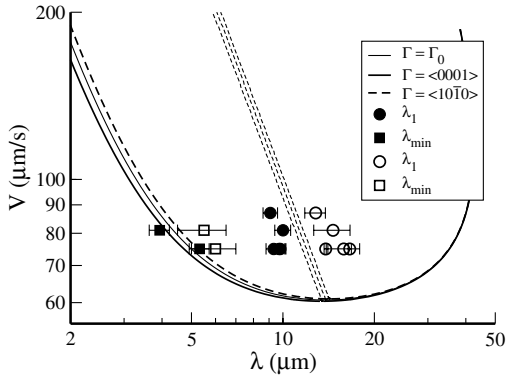

Fig. 6. Experimental data for λ_1 and λ_{min} obtained during the destabilization of planar front in different grains. The values are located in the stability map of Fig. 5, in the low velocity zone.

dilute alloys [6,7]. Also for both sets, the relation between λ_1/λ_{min} remains close to the $\lambda_{\sigma_{max}}/\lambda_0^-$ that can be obtained from the stability map for this system.

From the analysis of the experimental data and the stability map in Figs. 5 and 6, it can be seen that the incorporation of the angular dependence in surface tension shows the same deviation as was experimentally observed, but it is not enough to explain the full deviation. This difference could have a relation not only to the surface energy anisotropy, but also to a kinetic attachment effect. Another possibility could be that the value used for ϵ_0, which is typical value for fcc crystals, would be underestimated for our hcp system and must be evaluated or measured for this geometry by other means. Following Eq. (2), a greater value of ϵ_0 will not change the geometry in Fig. 2, but will show a more important deformation of the spherical surface given by Γ_0 and thus a greater difference in Figs. 5 and 6.

6. Conclusions

In this work, the stability of a planar solidification front of an hcp: Zn–0.01%Cd alloy directionally grown was studied. Experimentally, we found that the critical values λ_c and V_C depend on the growth direction. For this reason, the scope of the morphological stability theory was analyzed. In the original form, this theory does not incorporate the anisotropy contribution of the surface energy. By adding an angular dependence in this term, this model shows a shift for primary spacing (actually the $\lambda_{\sigma_{max}}$ value), as for λ_0^-, which corresponds to the minimal wavelength that could appear during the destabilization.

Although the application of the model shows a minor displacement for the critical velocity V_C, the difference is more notable for higher growth velocities, and also, as it can be expected for the smaller wavelengths, due to the square inverse dependence on λ of the capillary term.

Finally, the experimentally observed difference is greater than that expected for this correction. The reason could be that the value of the ϵ_0 for this system may be underestimated. As a first step, we used the typical value for metallic systems, but it would be interesting to calculate or measure it by other means.

Acknowledgements

This work was carried out at the IFIMAT (Instituto de Física de Materiales Tandil) and has partial support from CICPBA (Comisión de Investigaciones Científicas de la Provincia de Buenos Aires), CONICET (Consejo Nacional de Investigaciones Científicas y Técnicas) and SeCAT-UNCPBA (Secretaría de Ciencia, Arte y Tecnología de la Universidad Nacional del Centro de la Provincia de Buenos Aires).

References

[1] Boettinger WJ, Coriell S, Greer A, Karma A, Kurz W, Rappaz M, et al. Acta Mater 2000;48:43–70.
[2] Sekerka RF. Physica D 1984;12:212–4.
[3] Coriell SR, McFadden GB, Sekerka RF. J Cryst Growth 1990;100:459–66.
[4] Coriell SR, McFadden GB. Morphological Stability. In: Hurle DT, editor. Handbook of crystal growth. Amsterdam: Elsevier; 1993. p. 785–857.
[5] Biloni H, Boettinger WJ. Solidification. In: Physical metallurgy. Amsterdam: Elsevier; 1996. p. 669–842.
[6] Fornaro O, Palacio HA, Biloni H. In: Rappaz M, Beckermann C, Trivedi R, editors. Solidification processes and microstructures. A symposium in honor to Wilfried Kurz. Warrendale (PA): TMS; 2004. p. 219–24.
[7] Fornaro O, Palacio HA, Biloni H. Mater Sci Eng A 2005;417:134–42.
[8] Biloni H, di Bella R, Bolling GF. Trans Metall Soc AIME 1967;239:2012–9.
[9] Audero MA, Biloni H. J Cryst Growth 1972;12:297–308.
[10] Audero MA, Biloni H. J Cryst Growth 1973;18:257–64.
[11] Golovin A, Davis S. Physica D 1998;116:363–91.
[12] Liu S, Napolitano RE, Trivedi R. Acta Mater 2001;49:4271–6.
[13] Hoyt J, Asta M, Karma A. Phys Rev Lett 2001;86:5530–3.
[14] Cahn JW, Han SC, McFadden GB. J Stat Phys 1999;95:1337–60.
[15] Smithells CJ, Brandes EA, editors. Metals reference book. 5th ed. London: Butterworth Inc.; 1978.
[16] Fornaro O, Palacio HA. Scripta Metall Mater 1994;31:1265–70.
[17] Fornaro O, Palacio HA. Scripta Mater 1997;36:439–45.
[18] Fornaro O, Palacio HA, Biloni H. Mater Res Soc 1998;481:21–6.
[19] Biloni H, Bolling GF, Domian HA. Trans Metall Soc AIME 1965;233:1926.
[20] Flemings MC. Solidification processing. New York: McGraw-Hill; 1974.
[21] Trivedi R, Kurz W. Acta Metall 1986;34:1663–70.